# Propagating modes in subwavelength cylindrical holes

Peter B. Catrysse,[a] Hocheol Shin, and Shanhui Fan
*Department of Electrical Engineering, Edward L. Ginzton Laboratory, Box N-126, Stanford University, Stanford, California 94305-4088*

(Received 2 June 2005; accepted 2 October 2005; published 1 December 2005)

We analyze subwavelength cylindrical holes in an optically thick metallic film with the metal described by a plasmonic model. We emphasize that such holes always support propagating modes near the surface plasmon frequency, *regardless of how small the holes are*. Based on this analysis, we design both single holes and hole arrays in which propagating modes play a dominant role in the transport properties of incident light. These structures exhibit a region of operation that to the best of our knowledge has not been probed yet experimentally, while featuring a high packing density and diffraction-less behavior. © *2005 American Vacuum Society.* [DOI: 10.1116/1.2130344]

The optical properties of nanoapertures in an optically thick metallic film have been intensely researched in the past several years due to their fundamental importance in near-field optics and their practical significance to photonic devices and applications, including filters, near-field probes, and optical data storage.[1] It is well-known that the transmission characteristics are strongly influenced by the presence or absence of propagating modes inside the apertures.[2,3] In metallic nanoslits, enhanced transmission has been attributed to propagating transverse magnetic (TM) modes inside the slits.[2,4–8] For cylindrical holes, such as those used in the Ebbesen *et al.* original experiments,[9] the spectral features have been shown to be largely independent of the material used for the vertical walls of the hole.[10,11] Therefore, the prevailing wisdom is that cylindrical holes do not support propagating modes when the hole diameter is smaller than $\approx\lambda/2n_0$, where $\lambda$ is the wavelength of incident light and $n_0$ is the refractive index of the material inside the hole.[12,13] Instead, enhanced transmission is commonly associated with an excitation of surface wave resonances on the front and back surfaces of the metallic film and an evanescent tunneling process, through the holes, between these resonances.[9,11,13–16]

The absence of propagating modes for small holes, however, is only true when one assumes a perfect electric conductor (PEC) model for metal. At optical wavelengths, metals do not behave as a PEC and a more realistic material model is required to capture their optical properties.[17,18] For a cylindrical hole, it has been shown that the dispersion relation is qualitatively different from a PEC waveguide when a more realistic plasmonic model is assumed.[19] To the best of our knowledge, however, the importance of such dispersion relation for transport of incident light through cylindrical holes has never been recognized.

In this article, we present an analysis of the dispersion relation for subwavelength cylindrical holes in an optically thick metallic film when a plasmonic model is used to describe the metal. We emphasize that such holes always support propagating modes near the surface plasmon frequency, *regardless of how small the holes are*. When material losses are included as part of the plasmonic model, these modes still propagate over several microns, even when the radii of the holes are much smaller than $\approx\lambda/2n_0$. Based on this analysis, we use three-dimensional (3D) finite-difference time-domain (FDTD) simulations to design both single holes and hole array structures in which propagating modes play a dominant role in the transport properties of incident light. These structures feature a high packing density, diffraction-less behavior, and they exhibit a region of operation that to the best of our knowledge has not been probed yet experimentally.

To calculate the propagating modes inside a cylindrical hole, we consider a $z$-invariant waveguide with a cylindrical cross section of radius $r_0$ in the transverse $xy$ plane (Fig. 1 inset). For the dielectric inside the hole, we use a real, frequency-independent dielectric function $\epsilon_1$. For the surrounding metal, we define a complex, frequency-dependent dielectric function $\epsilon_2$. The waveguide mode $(m,n)$ is found by solving Maxwell's equations in cylindrical coordinates for electric and magnetic fields of the form $\psi(r,\phi,z,t)=\psi_n(r)\exp(jm\phi)\exp[j(\omega t-k_z z)]$, where $m$ is an integer denoting angular momentum, $n$ is related to the number of nodes in the radial direction, while $\omega$ and $k_z$ are the frequency and wave number of a mode in the hole, respectively. By matching boundary conditions, a transcendental equation is obtained for the dispersion relation[20]

$$\left[\frac{\epsilon_1}{k_{T,1}}\frac{J_m'}{J_m}-\frac{\epsilon_2}{k_{T,2}}\frac{H_m^{(1)\prime}}{H_m^{(1)}}\right]\left[\frac{1}{k_{T,1}}\frac{J_m'}{J_m}-\frac{1}{k_{T,2}}\frac{H_m^{(1)\prime}}{H_m^{(1)}}\right]=m^2\frac{c^2k_z^2}{\omega^2r_0^2}\left(\frac{1}{k_{T,1}^2}-\frac{1}{k_{T,2}^2}\right)^2, \tag{1}$$

where $J_m(k_{T,1}r)$ and $H_m^{(1)}(k_{T,2}r)$ represent $m$th-order Bessel and Hankel functions of the first kind, and

$$k_{T,i}=\sqrt{\left(\frac{\omega}{c}\right)^2\epsilon_i-k_z^2}\quad i=1,2. \tag{2}$$

The prime above these cylindrical functions denotes differentiation with respect to their argument. The speed of light in

[a]Author to whom correspondence should be addressed; electronic mail: pcatryss@stanford.edu

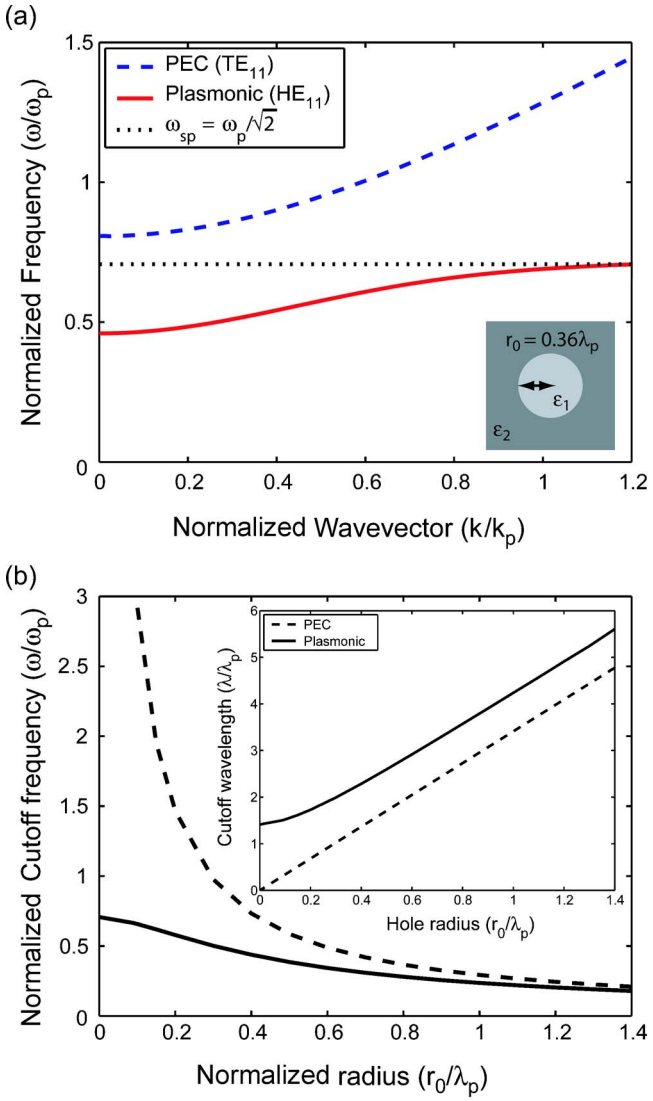


FIG. 1. (a) Dispersion relation of the lowest-order waveguide mode of a cylindrical hole in metal. The dashed blue line corresponds to the $TE_{11}$ mode in a perfect electric conductor (PEC). The solid red line corresponds to the $HE_{11}$ mode in a Drude plasmonic metal. The radius of the hole is $0.36\lambda_p$, where $\lambda_p$ is the plasmonic wavelength in the Drude model. (b) Cutoff frequency of the lowest-order waveguide mode vs hole radius $r_0$ for PEC ($TE_{11}$, dashed line) and plasmonic ($HE_{11}$, solid line) model.

vacuum is denoted by $c$. This dispersion equation differs qualitatively from that of a cylindrical PEC waveguide with radius $r_0$, for which $J_m'(k_{T,1}r_0)=0$ for transverse electric (TE) and $J_m(k_{T,1}r_0)=0$ for TM modes.[21]

In modeling apertures (slits and holes), it is quite common to use a PEC model to describe the surrounding metal.[2,4,22,23] At optical wavelengths, however, the optical properties of the metal differ significantly from the PEC model. Here, we use a Drude plasmonic model

$$\epsilon_2(\omega) = 1 - \frac{\omega_p^2}{\omega(\omega - i\omega_\tau)}, \tag{3}$$

where $\omega_p$ is the plasma frequency and $\omega_\tau$ is the collision frequency. This model takes into account the contribution of free electrons to the dielectric constant of metals. Despite its apparent simplicity, the plasmonic model proves to be a good approximation for noble metals (e.g., silver, gold, copper) and aluminum in the infrared regime. Moreover, by allowing for additional Lorentzian resonance terms its use can be easily extended to the visible wavelength range where interband transitions often contribute to the dielectric function.[18,19]

The propagating modes inside the cylindrical hole are obtained by solving for the roots of the dispersion equation Eq. (1). We numerically scan the normalized $(\omega, k_z)$ space for pairs that satisfy the dispersion equation. Figure 1(a) compares the dispersion behavior of the fundamental $TE_{11}$ mode in a PEC waveguide with the $HE_{11}$ mode in a lossless plasmonic waveguide. Both modes couple to incident plane waves, while next higher-order modes do not. We use as hole radius $r_0=0.36\lambda_p$, where $\lambda_p=2\pi c/\omega_p$ is the plasma wavelength. The collision frequency $\omega_\tau$ is set to zero. In the PEC case (dashed blue line), the fundamental $TE_{11}$ mode cuts off at $\omega_c^{TE_{11}}=0.292\pi c/r_0=0.81\omega_p(\lambda_c^{TE_{11}}=3.41r_0=1.24\lambda_p)$. Below this cutoff frequency, no propagating modes exist for a PEC waveguide.[21] The solid red line in Fig. 1(a) represents the dispersion of the fundamental $HE_{11}$ mode in the plasmonic waveguide, which has a normalized cutoff frequency $\omega_c=0.46\omega_p(\lambda_c=2.17\lambda_p)$. The cutoff wavelength of the $HE_{11}$ mode in the plasmonic waveguide is almost twice as long as the cutoff wavelength of the $TE_{11}$ mode in the PEC waveguide. Hence, the plasmonic waveguide can sustain a propagating mode at a significantly longer cutoff wavelength than is to be expected from a PEC waveguide model. Moreover, the qualitative difference in dispersion becomes particularly prominent for small holes. Figure 1(b) describes the evolution of the cutoff frequency (main panel) and wavelength (inset) for the fundamental mode as a function of hole radius for the PEC (dashed lines) and the plasmonic (solid lines) waveguide, respectively. For the PEC waveguide, the cutoff wavelength is proportional to the hole radius $r_0$ and approaches zero for small holes. For the plasmonic waveguide, two different regimes of operation can be seen. In the "large" hole regime, the behavior is quite similar to the PEC waveguide and differs only by a "fixed" offset in wavelength, which is approximately equal to $\lambda_p$. In the "small" hole region, however, the behavior of the plasmonic waveguide deviates significantly from the PEC result and the cutoff wavelength tends toward the surface plasmon wavelength $(\sqrt{2}\lambda_p)$ when the hole radius goes to zero. This suggests that cylindrical holes in a plasmonic material can support propagating modes near the surface plasmon frequency, regardless of how small are the holes. [Note that for holes that are sufficiently small, one needs to take into account the nonlocal nature or spatial dispersion of the complex dielectric function $\epsilon_2(\omega,k)$, i.e., the plasmonic model is no longer valid.[24] However, for holes larger than 100 nm, we still expect the local dielectric function to be valid.[19]]

Based upon the modal analysis above, we now consider the transport properties of a single hole and a hole array. In both cases, we assume a metal film with finite thickness $h$. We use a 3D total-field/scattered-field FDTD implementation

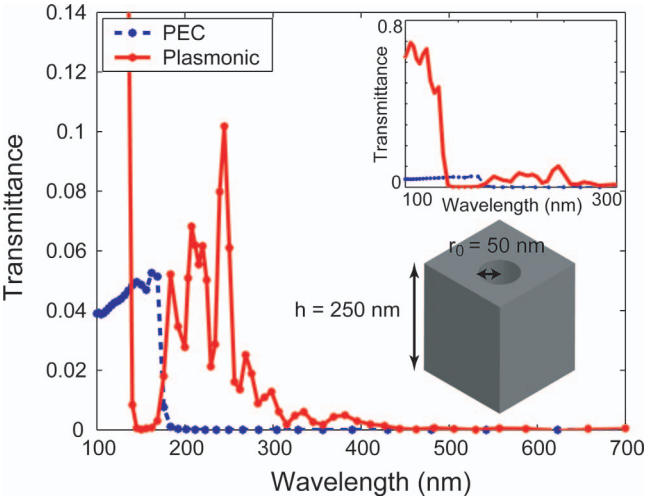


FIG. 2. Solid red line corresponds to the transmission spectrum of a single cylindrical hole ($r_0$=50 nm=0.36$\lambda_p$) in a 250 nm thick metal film as shown in the inset. The metal is modeled as a plasmonic material with $\lambda_p$ =138 nm ($\omega_p$=1.37×10$^{16}$ rad/s) and $\omega_\tau$=7.29×10$^{13}$ rad/s. The dashed blue line is the transmission spectrum for the same geometry, except that the metal is modeled as a PEC. The inset shows the transmission spectrum from 100 to 300 nm.

in which uniaxial phase-matched layer (UPmL) absorbing boundaries truncate the simulation domain. For the single hole simulation, we apply a normally incident pulsed Gaussian-beam excitation centered at 550 nm to obtain the response in the ultraviolet and visible wavelength range within a single simulation. The Gaussian beam has a transverse spatial full width half maximum of 1 $\mu$m. The incidence plane is chosen a few 100 nm above the metallic film and the field data for determining the spectral transport properties of the waveguide, through direct integration of the Poynting vector, are collected in an observation plane placed in the middle of the metallic film. Such calculation measures the total amount of power that can pass through the hole. The transmittance is defined as the ratio of the power through the waveguide in the metallic film to the incident power.

Figure 2 shows the spectral transmittance of a cylindrical hole ($r_0$=50 nm=0.36$\lambda_p$) in a 250 nm thick metal film, modeled as a PEC (dashed blue line) and a plasmonic material (solid red line), respectively. For the plasmonic material, we assume a plasma wavelength $\lambda_p$=138 nm [$\omega_p$=1.37×10$^{16}$ rad/s (Ref. 17] and $\omega_\tau$=7.29×10$^{13}$ rad/s.[18] The presence of a nonzero collision frequency leads to losses and we can calculate the decay length $L_d=1/2k_z''$, using the complex wave number of the mode $k_z=k_z'+ik_z''$. The decay length is approximately 2–3 $\mu$m for most of the wavelength range covered by the $HE_{11}$ mode. Hence, the $HE_{11}$ mode can propagate over a distance that is relevant for transport through metallic films, which are a few hundred nanometers thick. (The same conclusion holds when using tabulated data for the dielectric function of silver.[25])

In the PEC case, the spectral transmittance is approximately constant and then falls off at the cutoff wavelength $\lambda_c^{TE_{11}} \cong 3.41 r_0 = 170$ nm, which is determined by the radius of the hole only. In the plasmonic case, using the Drude free-electron model in Eq. (4) including losses, the transmittance depends on a combination of hole geometry and material properties. It features a region of high transmission below the bulk plasma wavelength ($\lambda_p$=138 nm), where the metal itself is transparent. This region is followed by a very fast dropoff leading to a stop band ranging from 150 to 200 nm. Past the stop band, a pass band with a cutoff located at $\lambda_c^{HE_{11}}$=300 nm is visible. Both the stop band and the cutoff wavelength compares well with the values obtained from the dispersion calculation. In comparison with the PEC case the pass band lies entirely beyond the PEC cutoff. The peak amplitude of the transmittance is twice as large as the peak amplitude in the PEC case. Its cutoff wavelength $\lambda_c^{HE_{11}}$ is almost twice as large as $\lambda_c^{TE_{11}}$ and features a decaying tail. Simulations without loss component in the plasmonic model revealed that the transmission spectrum is quasi-independent of material losses (mean difference <10%). This is consistent with long decay lengths, which are on the order of microns for the plasmonic model, compared to the 250 nm thickness of the film.

The importance of propagating modes on the transmission properties of subwavelength cylindrical holes is also evident for appropriately designed hole array structures. Previously, transmission enhancement for such structures has been largely associated with the resonant excitation of surface waves and evanescent tunneling through the holes.[9,11,13–16] Here, instead, we explore a different regime in which the propagating waveguide mode provides the dominant transport mechanism. For simplicity, we consider only plane waves incident along the normal direction. The signature of a propagating waveguide mode in the transmission will be most noticeable when the $HE_{11}$ band covers a wavelength range where no other competing mechanisms are present. Hence, the wavelengths of a surface wave resonance at normal incidence, due to the folding of the dispersion curve of the top and bottom surfaces,[9] should be below the smallest wavelength of the $HE_{11}$ band, which corresponds to the surface plasmon wavelength inside the hole. For this to occur, the array needs to have a periodicity that is substantially smaller than what has been featured in recent experiments. Furthermore (while this is not strictly necessary), to expand the propagating mode band to longer wavelengths, we fill the holes with a dielectric to achieve a large index contrast between the material inside the holes and the material surrounding metallic film. Figure 3 shows the transmittance spectrum $T$ for an array of cylindrical holes, which has been designed according to aforementioned principles. It features 50 nm radius cylindrical holes in a 250 nm thick metal film. The holes are filled with a dielectric with refractive index $\epsilon_1$=4 (e.g., $Si_3N_4$), while the periodicity of the array is 180 nm. For the PEC model, this array has a transmission spectrum with a cutoff wavelength of 370 nm, which is close to the cutoff wavelength for a single dielectric-filled hole. Below that wavelength, the transmission band features a series of high-finesse Fabry-Pérot resonances. In contrast, the spectrum of the plasmonic model shows a clear pass band ranging from 350 to 600 nm that lies entirely beyond the

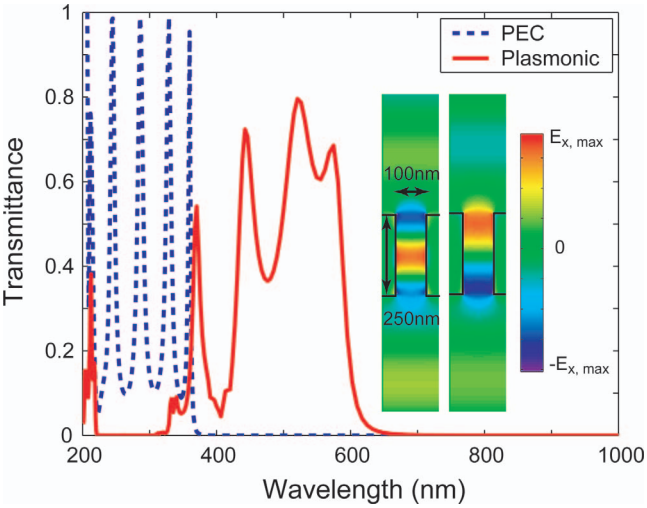


FIG. 3. Solid red line corresponds to the transmission spectrum $T$ of a 50 nm radius cylindrical hole array with 180 nm period (in $x$ and $y$) in a 250 nm thick metal film. The holes have been filled with a dielectric ($\epsilon_1=4$). The substrate and superstrate are air ($\epsilon_0=1$). Insets show $E_x$ field profile inside the hole for the two major peaks at wavelengths 442 nm ($T=0.72$, left panel) and 520 nm ($T=0.79$, right panel), respectively, with light incident from the top (The simulation domain used in 3D FDTD is $180\times180\times1000$ nm). The field pattern clearly shows the existence of propagating modes. The dashed blue line is the transmission spectrum for the same geometry, except the metal is modeled as a PEC.

PEC cutoff wavelength. This range, as well as the stop band between 220 and 320 nm, once more agrees well with the dispersion relation of a single hole. The insets show the $E_x$ field profile inside the aperture for the peaks at wavelengths 442 nm ($T=0.72$, left panel) and 520 nm ($T=0.79$, right panel). The field pattern clearly demonstrates the existence of propagating modes.

Making subwavelength apertures for use at optical wavelengths, as described in this work, requires features on the order of 50 nm. Recent experiments have shown that this is indeed possible.[26] In addition, we note that the transmission spectra reported here largely depend on material parameters rather than the exact shape of the cylindrical hole. Specifically, the upper frequency edge of the $HE_{11}$ pass band is pinned at the surface plasma frequency of the metal-dielectric interface inside the hole. Hence, its location depends on material properties only. Therefore, the presence of a transmission peak should be fairly robust against any disorders introduced during fabrication.

To the best of our knowledge, this work identifies an operating regime for cylindrical hole arrays. Our results show the potential of using propagating modes to obtain high transmission with subwavelength holes. In Fig. 3, the plasmonic pass band features a peak transmission of 0.79, which is approximately an order of magnitude higher when compared with previously published transmission in hole arrays. The use of small periodicity (approximately 200 nm) means that for all wavelengths of practical interest the array is diffraction-free while allowing for a bigger packing density of holes and potentially a smaller footprint.

This work was supported in part by National Science Foundation Grant No. ECS-0134607 and by AFOSR Grant No. FA9550-04-1-0437. H.S. acknowledges the support of the Samsung Lee Kun Hee fellowship.

[1]For the latest developments, see, for example, the focus issue in Opt. Express **12**, 3618 (2004).
[2]J. A. Porto, F. J. Garcia-Vidal, and J. B. Pendry, Phys. Rev. Lett. **83**, 2845 (1999).
[3]F. I. Baida and D. Van Labeke, Phys. Rev. B **67**, 155314 (2003).
[4]Y. Takakura, Phys. Rev. Lett. **86**, 5601 (2001).
[5]E. Popov, M. Neviere, S. Enoch, and R. Reinisch, Phys. Rev. B **62**, 16100 (2000).
[6]S. Astilean, P. Lalanne, and M. Palamaru, Opt. Commun. **175**, 265 (2000).
[7]P. Lalanne, J. P. Hogonin, S. Astilean, M. Palamaru, and K. D. Moller, J. Opt. A, Pure Appl. Opt. **2**, 48 (2000).
[8]Q. Cao and P. Lalanne, Phys. Rev. Lett. **88**, 057403 (2002).
[9]T. W. Ebbesen, H. J. Lezec, H. F. Ghaemi, T. Thio, and P. A. Wolff, Nature (London) **391**, 667 (1998).
[10]D. E. Grupp, H. J. Lezec, T. W. Ebbesen, K. M. Pellerin, and T. Thio, Appl. Phys. Lett. **77**, 1569 (2000).
[11]L. Martin-Moreno, F. J. Garcia-Vidal, H. J. Lezec, K. M. Pellerin, T. Thio, J. B. Pendry, and T. W. Ebbesen, Phys. Rev. Lett. **86**, 1114 (2001).
[12]W. L. Barnes, W. A. Murray, J. Dintinger, E. Devaux, and T. W. Ebbesen, Phys. Rev. Lett. **92**, 107401 (2004).
[13]W. L. Barnes, A. Dereux, and T. W. Ebbesen, Nature (London) **424**, 824 (2003).
[14]A. Krishnan, T. Thio, T. J. Kima, H. J. Lezec, T. W. Ebbesen, P. A. Wolff, J. Pendry, L. Martin-Moreno, and F. J. Garcia-Vidal, Opt. Commun. **200**, 1 (2001).
[15]J. B. Pendry, L. Martin-Moreno, and F. J. Garcia-Vidal, Science **305**, 847 (2004).
[16]H. J. Lezec and T. Thio, Opt. Express **12**, 3629 (2004).
[17]M. A. Ordal, R. J. Bell, R. W. Alexander, Jr., L. L. Long, and M. R. Querry, Appl. Opt. **24**, 4493 (1985).
[18]A. D. Rakic, A. B. Djurisic, J. M. Elazar, and M. L. Majewski, Appl. Opt. **37**, 5271 (1998).
[19]L. Novotny and C. Hafner, Phys. Rev. E **50**, 4094 (1994).
[20]C. A. Pfeiffer, E. N. Economou, and K. L. Ngai, Phys. Rev. B **10**, 3038 (1974).
[21]D. M. Pozar, *Microwave Engineering* (Wiley, New York, 1997).
[22]F. de Abajo, Opt. Express **10**, 1475 (2002).
[23]F. J. Garcia-Vidal and L. Martin-Moreno, Phys. Rev. B **66**, 155412 (2002).
[24]G. C. Aers, A. D. Boardman, and B. V. Paranjape, J. Phys. F: Met. Phys. **10**, 53 (1980).
[25]E. D. Palik and G. Ghosh, *Handbook of Optical Constants of Solids* (Academic, Orlando, 1985).
[26]J. A. Matteo, D. P. Fromm, Y. Yuen, P. J. Schuck, W. E. Moerner, and L. Hesselink, Appl. Phys. Lett. **85**, 648 (2004).